NEURAL REGENERATION RESEARCH
www.nrronline.org

Research Article

MicroRNA-101a-3p mimic ameliorates spinal cord ischemia/reperfusion injury

https://doi.org/10.4103/1673-5374.335164

Date of submission: June 22, 2021

Date of decision: September 9, 2021

Date of acceptance: November 10, 2021

Date of web publication: February 8, 2022

Zai-Li Zhang, Dan Wang, Feng-Shou Chen*

From the Contents

Graphical Abstract *MicroRNA-101a-3p mimic ameliorates spinal cord ischemia/reperfusion injury by inhibiting MYCN and the p53 signaling pathway*

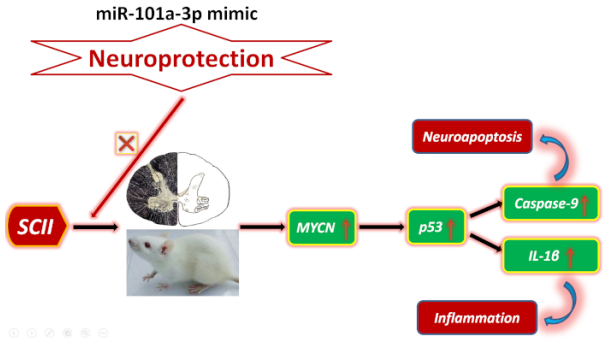

Abstract

miR-101a-3p is expressed in a variety of organs and tissues and plays a regulatory role in many diseases, but its role in spinal cord ischemia/reperfusion injury remains unclear. In this study, we established a rat model of spinal cord ischemia/reperfusion injury by clamping the aortic arch for 14 minutes followed by reperfusion for 24 hours. Results showed that miR-101a-3p expression in L4–L6 spinal cord was greatly decreased, whereas MYCN expression was greatly increased. Dual-luciferase reporter assay results showed that miR-101a-3p targeted MYCN. MYCN immunoreactivity, which was primarily colocalized with neurons in L4–L6 spinal tissue, greatly increased after spinal cord ischemia/reperfusion injury. However, intrathecal injection of an miR-101a-3p mimic within 24 hours before injury decreased MYCN, p53, caspase-9 and interleukin-1β expression, reduced p53 immunoreactivity, reduced the number of MYCN/NeuN-positive cells and the number of necrotic cells in L4–L6 spinal tissue, and increased Tarlov scores. These findings suggest that the miR-101a-3p mimic improved spinal ischemia/reperfusion injury-induced nerve cell apoptosis and inflammation by inhibiting MYCN and the p53 signaling pathway. Therefore, miR-101a-3p mimic therapy may be a potential treatment option for spinal ischemia/reperfusion injury.

Key Words: apoptosis; caspase-9; inflammation; interleukin-1β; microRNA-101a-3p; MYCN; nerve cells; p53; spinal cord ischemia/reperfusion injury

Introduction

Clinical vascular malformation surgery and aortic aneurysm surgery can induce spinal cord ischemia/reperfusion injury (SCII) (Li et al., 2014b). Paraplegia is regarded as the most serious complication caused by SCII, and it imposes a significant economic and mental burden on patients and their families (Liu et al., 2017). The neuropathologic mechanism of SCII is complex and is not fully understood (Wang et al., 2017). Neuronal damage is associated with lower limb motor dysfunction, and it is challenging to repair nerve function after SCII. Therefore, our research team has been carrying out related studies on the mechanisms of neuronal damage (Li et al., 2018b). The present study focuses on neuroapoptosis and inflammation.

MicroRNAs (miRNAs) are single-stranded and non-coding RNAs that can modulate protein function by inhibiting mRNA translation (Khanna et al., 2013; Roshan et al., 2014). Multiple miRNAs have been shown to be changed after SCII, and changes in miRNA can simultaneously regulate neuroapoptosis and inflammation upstream of mRNA translation and significantly affect the downstream response (Bao et al., 2018). For example, an miR-129-5p mimic ameliorated blood-spinal cord barrier damage and neuroinflammation through restraining high-mobility group box-1 (Li et al., 2017), and miR-320 knockdown has been shown to exert neuroprotection against SCII (He et al., 2015). Of multiple miRNAs, miR-101a-3p has attracted increasing attention. miR-101a-3p is expressed in various organs and tissues and plays a regulatory role in many diseases. Overexpression of miR-101a-3p has been shown to attenuate amyloid precursor protein-induced Alzheimer's disease (Lin et al., 2019). Additionally, miR-101a-3p has been shown to suppress the fibrosis of trans-aortic constriction and isolated cardiac fibroblasts (Zhou et al., 2018). Furthermore, miR-101a-3p promotes the differentiation of bone marrow cells into microglia and regulates the morphology and inflammatory response of microglia (Saika et al., 2017). Nevertheless, the mechanism of miR-101a-3p is still unknown. In the present study, we investigated the underlying mechanism of miR-101a-3p in SCII.

V-myc myelocytomatosis viral-related oncogene (MYCN) is a member of the MYC family of proto-oncogenes (Chava et al., 2020), which is crucially associated with multiple cancers, including glioblastoma (Korshunov et al., 2017), lung cancer (Peifer et al., 2012), and leukemia (Astolfi et al., 2014). It has been reported that MYCN modulates the cell cycle, cellular proliferation, DNA damage and

Department of Anesthesiology, the First Hospital of China Medical University, Shenyang, Liaoning Province, China
*Correspondence to: Feng-Shou Chen, MD, PhD, haoxiu19881988@126.com.
https://orcid.org/0000-0001-7897-8680 (Zai-Li Zhang)

How to cite this article: *Zhang ZL, Wang D, Chen FS (2022) MicroRNA-101a-3p mimic ameliorates spinal cord ischemia/reperfusion injury. Neural Regen Res 17(9):2022-2028.*

apoptosis (He et al., 2017), and plays a vital role in the CNS (Zindy et al., 2006). Aberrant expression of MYCN is closely related to hypoxic-ischemic encephalopathy (Jiang et al., 2018), indicating that MYCN may be involved in the occurrence and development of neurological diseases. Recently, multiple miRNAs have been shown to directly target MYCN expression in certain diseases. For example, miR-29b restrains the growth of glioma in an MYCN-dependent manner (Sun et al., 2017), and miR-34a regulates MYCN expression to exert an antitumor function (Wei et al., 2008). In particular, miR-101a-3p was downregulated in an SCII model using a previous miRNA analysis (Bao et al., 2018). However, the mechanism of miR-101a-3p and MYCN in SCII is not clear. Some studies have reported that MYCN regulates the p53 signaling pathway and mediates a key mechanism of apoptosis (Roy et al., 1994; Chen et al., 2010). This study aimed to investigate the role of miR-101a-3p in SCII and whether it functions by inhibiting MYCN and the p53 signaling pathway.

Materials and Methods

Animals

The 8-week-old male Sprague-Dawley rats (about 250 g, *n* = 76) were acquired from the Laboratory Animal Service Center of China Medical University (SCXK (Liao) 2015-0001) as previously reported (Li et al., 2014b, 2018b). The animals were allowed free water and chow in normative cages that were kept at 23°C and 50–60% relative humidity for at least 1 week before surgery. All experiments were designed and reported according to the Animal Research: Reporting of *In Vivo* Experiments (ARRIVE) guidelines (Percie du Sert et al., 2010). The animal study was reviewed and approved by the Animal Ethics Review Committee for Animal Experimentation of China Medical University (approval No. CMU2020267) on March 2, 2020. In initial experiments, 36 rats were sacrificed to measure the Tarlov scores and expression of miR-101a-3p and MYCN at various time points (12, 24, 36, and 48 hours) after SCII. For subsequent experiments, 40 rats were intrathecally injected with normal saline, synthetic miR-101a-3p mimic, negative control (NC) or inhibitor (eight rats in each group).

Surgical procedure

The SCII operation was performed as previously reported (Li et al., 2014b, 2018b). All animals were mechanically ventilated by endotracheal intubation after being anesthetized by intraperitoneal injection of 4% sodium pentobarbital (50 mg/kg; Beyotime Biotechnology, Shanghai, China). Then, the aortic arch was exposed via left anterior thoracotomy.

After exposing the aortic arch, an arterial clamp was placed between the left subclavian artery and left carotid artery. Efficient occlusion lasted for 14 minutes. After a 90% reduction of flow at the tail artery was confirmed with a Doppler monitor (Moor Instruments, Axminster, Devon, UK), the clamp was removed, followed by reperfusion for 24 hours. Sham-operated animals went through the same process without occlusion.

Neurological evaluation

At 24 hours after the surgery, hind limb function was evaluated using the Tarlov system with two observers blinded to the experiment. The Tarlov scoring system was performed as previously reported (Li et al., 2014a, c) with the following scores: 0 = no movement of hind limbs; 1 = weak detectable hind limb movement; 2 = some hind limb movement; 3 = abnormal standing and walking; 4 = normal hind limb motor function.

Real-time polymerase chain reaction

Rats were sacrificed after surgery with an overdose (100 mg/kg) of sodium pentobarbital. The total RNA from L4–L6 specimens of the spinal cord was obtained using the TRIzol agentia. Subsequently, complementary DNA was obtained after reverse transcription using the PrimeScript RT reagent kit with genomic DNA Eraser (RR047A, Takara, Otsu, Japan) and Mir-X™ miRNA First-Strand Synthesis Kit (638315, Takara). The complementary DNA of miR-101a-3p and MYCN was incubated with an SYBR Premix Ex TaqII kit (Takara) at 95°C (10 minutes), followed by 40 cycles at 95°C (20 seconds), 60°C (60 seconds), 62°C (30 seconds), and 72°C (30 seconds). U6 or glyceraldehyde-3-phosphate dehydrogenase (GAPDH) was included as the reference gene, and each reaction was measured with the $2^{-\Delta\Delta Ct}$ method (Li et al., 2017). The primers used were: miR-101a-3p (5′-TAC AGT ACT GTG ATA ACT GAA-3′), U6 (5′-CTC GCT TCG GCA GCA CA-3′, 5′-AAC GCT TCA CGA ATT TGC GT-3′), MYCN (5′-ACC CAA CAT CAG CGG TCG-3′, 5′-CGT GAC TGT CGG GTT TTC CA-3′), GAPDH (5′-GGG GCT CTC TGC TCC TCC CTG-3′, 5′-AGG CGT CCG ATA CGG CCA AA-3′).

Western blot assay

The MYCN-mediated p53 signaling pathway protein was detected by western blot assay. Rats were sacrificed after surgery with an overdose of sodium pentobarbital (100 mg/kg). The L4–L6 segments were prepared in lysis buffer on ice and separated at 4°C, and total proteins were collected in the supernatants as previously reported (Li et al., 2014c). The proteins were purified with a protein extraction kit (Beyotime, Shanghai, China). Following electrophoresis and membrane transfer, the membranes were sealed and incubated at 4°C overnight with the following antibodies: MYCN (rabbit, Cat# 13987, 1:1000, RRID: AB_2631168, Cell Signaling Technology, Boston, MA, USA), p53 (mouse, Cat# ab26, 1:200, RRID: AB_303198, Abcam, Cambridge, MA, USA), caspase-9 (mouse, Cat#9508, 1:1000, RRID: AB_2068620, Cell Signaling Technology), GAPDH (rabbit, Cat# AF7021, 1:5000, RRID: AB_2839421, Affinity Biosciences, Jiangsu, China), and IL-1β (rabbit, Cat# ab9722, 1:2500, RRID: AB_308765, Abcam). After being washed with Tris buffer solution-Tween 20, proteins were incubated with the appropriate secondary antibodies: anti-mouse (Cat# SA00001-1, 1:10,000, RRID: AB_2722565, Proteintech, Wuhan, China) or anti-rabbit (Cat# SA00001-2, 1:10,000, RRID: AB_2722564, Proteintech) at 37°C for 1 hour. A chemiluminescence kit (Bio-Rad, Philadelphia, PA, USA) and Quantity One software (Bio-Rad) were used to detect the optical densities. GAPDH served as a reference protein.

Intrathecal infusion

The synthetic miR-101a-3p mimic, negative control (NC) and inhibitor were obtained from GenePharma Company (Shanghai, China). The synthetic miR-101a-3p was transfected with Lipofectamine 3000 by intrathecal infusion using a 25-μL microsyringe (Gaoge Co, Ltd., Shanghai, China). The rat spinal cord does not typically extend below the fourth lumbar vertebra (Padmanabhan and Singh, 1979). The needle was placed between sections L4–L6 of the dura followed by a sudden tail flick, as previously described (Mestre et al., 1994; Wang et al., 2020a). Days and concentrations of intrathecal infusion were determined according to the results of a preliminary experiment. Three consecutive intrathecal infusions were performed for the animals before surgery with intervals of 24 hours, and the SCII operation was performed at 24 hours after the last injection. Each infusion included 20 μL of miR-101a-3p mimic, NC or inhibitor with a concentration of 3.3 μg/μL. Normal saline (20 μL) was injected into the sham and SCII groups. Only the rats with normal motor function (Tarlov score = 4) after intrathecal infusion were included in the study. The sequences of the miR-101a-3p mimic, miR-101a-3p inhibitor and miR-101a-3p NC were: (5′-UAC AGU ACU GUG AUA ACU GAA-3′, 5′-CAG UUA UCA CAG UAC UGU AUU-3′), (5′-UUC AGU UAU CAC AGU ACU GUA-3′), and (5′-UUC UCC GAA CGU GUC ACG UTT-3′, 5′-ACG UGA CAC GUU CGG AGA ATT-3′), respectively.

Dual-luciferase reporter assay

The potential binding site between miR-101a-3p and MYCN was predicted by the TargetScan 7.2 database (http://www.targetscan.org/vert_72/). The direct interaction between miR-101a-3p and MYCN was determined by a luciferase assay as previously reported (Le et al., 2011). Briefly, 293T cells (CL-0005, Procell Biotechnology, Wuhan, China) were transfected with the miR-101a-3p mimic or NC, and a luciferase reporter vector containing the wild-type (WT; 5′-GAA GUU CAC ACC UAA GUA CUG UA-3′) or mutant (MUT; 5′-GAA GUU CAC ACC UAA UGC AGU GA-3′) by X-tremeGENE HP (Roche, Hilden, Germany). At 48 hours after the transfection, luciferase activity was measured with a Luciferase Assay Kit (Promega Corp., Madison, WI, USA). The ratio between firefly and renilla was calculated to normalize the relative luciferase activity.

Immunofluorescence staining

The distribution of MYCN and p53 after SCII were measured by immunofluorescence staining at 24 hours. After fixation with paraformaldehyde and dehydration with alcohol, the spinal cord L4–L6 specimens were embedded with paraffin and sectioned into 4-μm segments with a microtome. Then, the 4-μm segments were sealed with 10% bovine serum albumin at 37°C for 2 hours after the

deparaffinization and antigen retrieval. The sealed segments were incubated at 4°C overnight with primary antibodies: rabbit anti-MYCN (Cat# 13987, 1:200, RRID: AB_2631168, Cell Signaling Technology), mouse anti-p53 (Cat# ab26, 1:100, RRID: AB_303198, Abcam), mouse anti-NeuN (neuronal marker [Wang et al., 2020b], Cat# ab104224, 1:400, RRID: AB_10711040, Abcam), goat anti-GFAP (astrocyte marker [Wang et al., 2020b], Cat# ab53554, 1:400, RRID: AB_880202, Abcam), and mouse anti-Iba-1 (microglial marker [Wang et al., 2020b], Cat# ab5076, 1:400, RRID: AB_2224402, Abcam). After being washed with phosphate buffered saline solution, the segments were incubated at 37°C for 1 hour with fluorescein-donkey anti-mouse IgG (H+L) (Cat# SA00003-9, 1:200, RRID: AB_2857366, Proteintech), Alexa Fluor 594-donkey anti-rabbit IgG (H+L) (Cat# SA00013-8, 1:200, RRID: AB_2857367, Proteintech) and fluorescein-donkey anti-goat IgG (H+L) (Cat# SA00003-3, 1:200, RRID: AB_2857365, Proteintech). A fluorescence microscope (Lycra Microsystems, Buffalo Grove, IL, USA) was used to capture representative images in the gray matter of the spinal anterior horn after covering the sections with anti-fluorescent quenchers. The quantitative analysis was performed using ImageJ software (NIH, Bethesda, MD, USA; Wang et al., 2020a).

Terminal deoxynucleotidyl transferase dUTP nick end labeling assay

Terminal deoxynucleotidyl transferase dUTP nick end labeling (TUNEL) is widely used to detect cell apoptosis by DNA fragments (Li et al., 2018a). First, the spinal cord L4–L6 tissues were sectioned into 8-μm segments by a microtome. After that, the segments were stained using a TUNEL Apoptosis Detection Kit (Servicebio, Wuhan, China). After being labeled with 4′,6-diamidino-2-phenylindole (Servicebio), the segments were examined in the gray matter of the spinal anterior horn under a TCS SP2 fluorescence microscope (Lycra Microsystems). Cells double-labeled with 4′,6-diamidino-2-phenylindole (blue) and TUNEL (red) were regarded as TUNEL-positive cells and counted by two observers blinded to each other. The averages of three sections per rat were analyzed to compare the differences between groups.

Statistical analysis

No statistical methods were used to predetermine sample sizes; however, our sample sizes are similar to those reported in previous publications (Wang et al., 2020a). Ten rats were excluded for various reasons including technical difficulties or death. All obtained data were analyzed as the mean ± standard deviation (SD) by SPSS 25.0 (IBM Corp., Armonk, NY, USA) and GraphPad Prism 7.0 (GraphPad Software Inc., La Jolla, CA, USA). One- or two-way analysis of variance was used to analyze normally distributed data, and a Kruskal-Wallis test or Mann-Whitney *U* test was used for non-normally distributed data. A *P*-value < 0.05 was considered statistically significant.

Results

Abnormal expression of miR-101a-3p/MYCN and neurological function after SCII

The expression of miR-101a-3p and MYCN was evaluated by real-time polymerase chain reaction and western blot at different time points after SCII. As shown in **Figure 1A**, miR-101a-3p expression was the lowest in the SCII 24 hours group, which was significantly reduced compared with that in the sham group ($P < 0.05$). Moreover, mRNA and protein expression of MYCN increased over time and peaked in the SCII 24 hours group, and the values were significantly increased compared with those in the sham group ($P < 0.05$; **Figure 1B–D**).

On the basis of the previous results, we selected 24 hours as the time point for the following experiments. **Figure 1E** shows the evaluation of hind limb function by the Tarlov scoring system. Tarlov scores were greatly reduced in the SCII group compared with those in the sham group ($P < 0.05$). The changes in neurological assessment and in miR-101a-3p expression occurred at the same time point after SCII, suggesting a possible relationship between motor dysfunction and miR-101a-3p.

MYCN is a target of miR-101a-3p

The TargetScan 7.2 database predicted the possible binding site of miR-101a-3p to be the 3′ untranslated region (UTR) of MYCN (**Figure 2A**). Intrathecal injection of the synthetic miR-101a-3p mimic increased miR-101a-3p expression and reduced MYCN expression compared with those in the SCII group ($P < 0.05$; **Figure 2B** and **C**). These results indicated a possible relationship between miR-101a-3p and MYCN, which we investigated further via a dual-luciferase reporter assay. The luciferase activity of the WT-3′UTR reporter was significantly reduced by transfection with the miR-101a-3p mimic ($P < 0.05$), whereas that of the MUT-3′UTR reporter was unchanged ($P > 0.05$; **Figure 2D** and **E**). Additionally, there were no obvious changes through the transfection with NC ($P > 0.05$; **Figure 2E**). Therefore, we ascertained that miR-101a-3p directly targets MYCN.

Cellular distribution of MYCN expression after SCII

Double immunofluorescence labeling of MYCN with NeuN, Iba-1 or GFAP was performed at 24 hours after SCII. As shown in **Figure 3A**, MYCN fluorescent signal was mainly colocalized with the NeuN fluorescent signal but not with GFAP or Iba-1 at 24 hours after SCII, suggesting that MYCN was at least partially upregulated in neurons. As shown in **Figure 3B**, the ratio of MYCN/NeuN double-positive cells was upregulated in the SCII group compared with that in the sham group ($P < 0.05$). Furthermore, the analysis showed that SCII increased the number of MYCN-labeled neurons ($P < 0.05$, *vs*. sham; **Figure 3C**).

miR-101a-3p improves hind limb motor function and inhibits MYCN levels in neurons after SCII

As shown in **Figure 4A**, the Tarlov scoring system was used to assess hind limb motor function after SCII as described in our previous research (Zhang et al., 2021). Tarlov scores in the SCII group and NC group were decreased at 24 hours after SCII compared with those in the sham group ($P < 0.05$). Tarlov scores in the SCII and NC groups were similar ($P > 0.05$). Tarlov scores in the miR-101a-3p mimic group were greatly upregulated compared with those in the SCII group ($P < 0.05$). The data demonstrate that the miR-101a-3p mimic ameliorated hind limb motor dysfunction after SCII.

As shown in **Figure 4B**, MYCN was colocalized with NeuN within the groups. The ratio and number of MYCN/NeuN double-positive cells in the miR-101a-3p mimic group were decreased at 24 hours after SCII compared with those in the SCII group ($P < 0.05$); whereas, there were no obvious differences between the SCII, NC and miR-101a-3p inhibitor groups ($P > 0.05$). Quantitative analysis in **Figure 4C** and **D** showed that SCII increased MYCN expression in neurons, which was then reduced by the miR-101a-3p mimic. These results suggested that the miR-101a-3p mimic might ameliorate SCII impairment by inhibiting MYCN expression in neurons.

miR-101a-3p decreases cell apoptosis after SCII

TUNEL assay was used to detect apoptotic cells in the spinal cord after SCII. As shown in **Figure 5A** and **B**, apoptosis rates in the SCII, NC, and miR-101a-3p inhibitor groups were greatly upregulated compared with that in the sham group ($P < 0.05$), and the apoptosis rate in the miR-101a-3p mimic group was greatly decreased compared with that in the SCII group ($P < 0.05$). These results demonstrated that the miR-101a-3p mimic ameliorated cell apoptosis after SCII.

Protection by miR-101a-3p against SCII through inhibiting the MYCN-p53-caspase9 signaling pathway and proinflammatory cytokine IL-1β production

The function of the miR-101a-3p mimic on modulating neuroapoptosis through the MYCN-p53-caspase9 signaling pathway was investigated with double immunofluorescence staining and western blot. Western blot showed that the protein expression levels of MYCN, p53 and caspase-9 were greatly increased in the SCII group compared with those in the sham group, and were greatly decreased in the miR-101a-3p mimic group compared with the SCII group ($P < 0.05$; **Figure 6A–D**). Proinflammatory cytokine IL-1β showed similar trend (**Figure 6A–E**). It can be concluded that the miR-101a-3p mimic protected against SCII by inhibiting proinflammatory cytokine IL-1β production.

As shown in **Figure 6F**, MYCN fluorescence was colocalized with p53 fluorescence at 24 hours after SCII. The quantitative analysis in **Figure 6G** and **H** show that the number of cells double-positive for MYCN and p53 in the miR-101a-3p mimic group were decreased compared with that in the SCII group ($P < 0.05$), and there were no obvious differences between the SCII, NC and miR-101a-3p inhibitor groups ($P > 0.05$). It can be concluded that the miR-101a-3p mimic reduced the expression of caspase-9 and thus protected against SCII by inhibiting the MYCN-p53-caspase-9 signaling pathway.

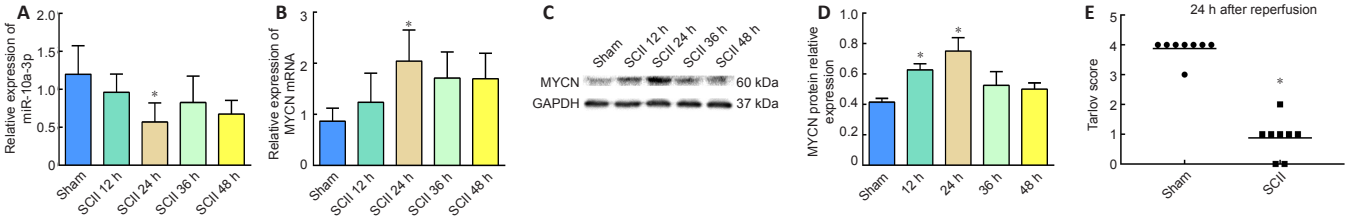

Figure 1 | Changes of miR-101a-3p/MYCN expression and neurological function after SCII.
(A, B) Quantification of MYCN and miR-101a-3p RNA expression within 48 hours after SCII. The relative expression of MYCN was normalized by GAPDH, and miR-101a-3p was normalized by U6. (C, D) Quantification of MYCN protein expression within 48 hours after SCII. The relative expression of MYCN was normalized by the reference protein GAPDH. (E) Neurological function was assessed by the Tarlov scoring system. The data are expressed as the mean ± SD (n = 8). *P < 0.05, *vs.* sham group (A, B, D: one-way analysis of variance; E: Mann-Whitney U test). GAPDH: Glyceraldehyde-3-phosphate dehydrogenase; MYCN: v-myc myelocytomatosis viral-related oncogene; SCII: spinal cord ischemia/reperfusion injury.

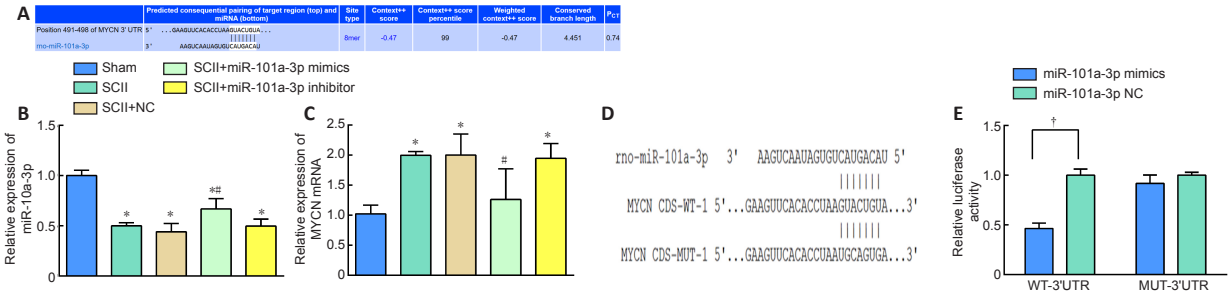

Figure 2 | MYCN is a target of miR-101a-3p.
(A) A possible binding site of miR-101a-3p was predicted to be the 3′UTR of MYCN by the TargetScan 7.2 database. (B, C) Synthetic miR-101a-3p was intrathecally injected to assess MYCN and miR-101a-3p RNA expression. The miR-101a-3p mimic effectively increased miR-101a-3p expression and reduced MYCN expression in comparison with the SCII group. The relative expression of MYCN was normalized by GAPDH, and miR-101a-3p was normalized by U6. The data are expressed as the mean ± SD (n = 4 in each group). *P < 0.05, *vs.* sham group; #P < 0.05, *vs.* SCII group (one-way analysis of variance). (D, E) A dual-luciferase assay confirmed the connection of miR-101a-3p and MYCN. The luciferase activity of the WT-3′UTR reporter was significantly reduced by transfection with the miR-101a-3p mimic, whereas that of the MUT-3′UTR reporter was unchanged. The data are expressed as the mean ± SD (n = 3). †P < 0.05, *vs.* NC group (two-way analysis of variance). 3′UTR: 3′Untranslated region; MUT: mutant; MYCN: v-myc myelocytomatosis viral-related oncogene; NC: negative control; SCII: spinal cord ischemia/reperfusion injury; WT: wild-type.

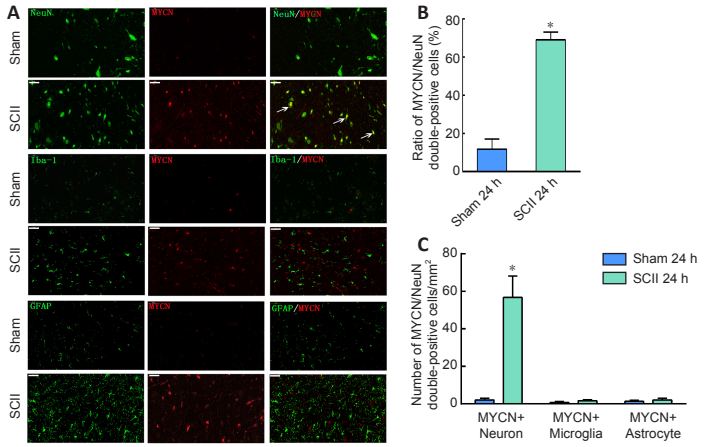

Figure 3 | Immunofluorescence assay of MYCN and cell markers at 24 hours after SCII.
(A) Cellular distribution of MYCN (red, Alexa Fluor 594) with GFAP (astrocyte marker; green, fluorescein), NeuN (neuronal marker; green, fluorescein) and Iba-1 (microglial marker; green, fluorescein). Colocalization was represented by yellow signals (white arrows). Compared with the sham group, the SCII group showed stronger MYCN immunoreactivity. Scale bar: 50 μm, original magnification, 40×. (B) Ratio of MYCN/NeuN double-positive cells. (C) Quantification of MYCN/NeuN double-positive cells. The data are expressed as the mean ± SD (n = 3). *P < 0.05, *vs.* sham group (two-way analysis of variance). GFAP: Glyceraldehyde 3-phosphate dehydrogenase; Iba-1:ionized calcium binding adapter molecule 1; MYCN: v-myc myelocytomatosis viral-related oncogene; NeuN: neuronal nuclei; SCII: spinal cord ischemia/reperfusion injury.

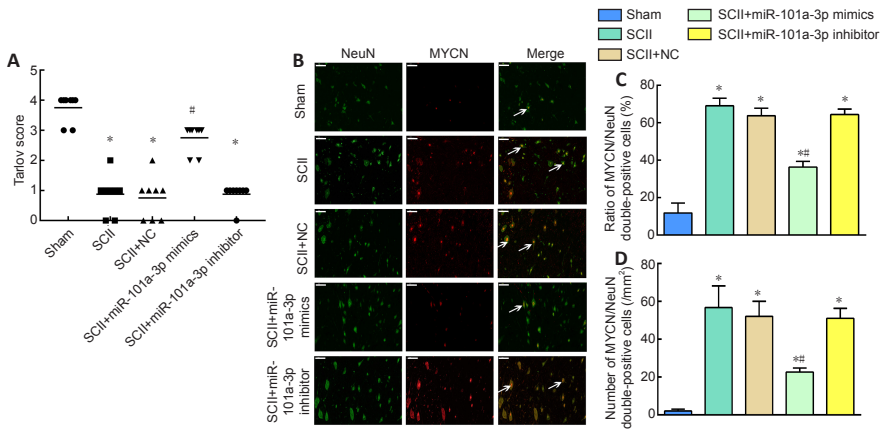

Figure 4 | The role of synthetic miR-101a-3p on hind limb motor function and MYCN fluorescence expression in neurons.
(A) The Tarlov scoring system was used to assess lower limb motor function after SCII with a range from 0 to 4. Each rat was represented by a different sign (n = 8). (B) Colocalization of MYCN (red, Alexa Fluor 594) and NeuN (green, fluorescein). Colocalization was represented by yellow signals (white arrows). Compared with the sham group, the SCII group showed stronger MYCN immunoreactivity, whereas immunoreactivity in the miR-101a-3p mimic group was decreased compared with that in the SCII group. Scale bars: 50 μm, original magnification, 40×. (C) The ratio of MYCN/NeuN double-positive cells (n = 3). (D) Number of MYCN/NeuN double-positive cells (n = 3). The data are expressed as the mean ± SD. *P < 0.05, *vs.* sham group; #P < 0.05, *vs.* SCII group (A: Mann-Whitney U test; B, D: one-way analysis of variance). MYCN: v-Myc myelocytomatosis viral-related oncogene; NC: negative control; NeuN: neuronal nuclei; SCII: spinal cord ischemia/reperfusion injury.

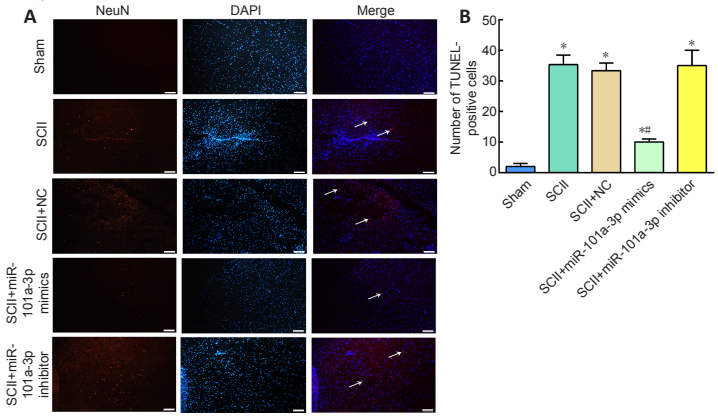

Figure 5 | The effect of synthetic miR-101a-3p on cell apoptosis at 24 hours after SCII.
(A) Micrographs of TUNEL (red) and DAPI (blue) in the anterior horn of the spinal cord. Compared with the sham group, the SCII group had a larger number of TUNEL-positive cells (white arrows), and the number in the miR-101a-3p mimic group was decreased compared with that in the SCII group. Scale bar: 100 μm. (B) Number of TUNEL-positive cells. The data are expressed as the mean ± SD (n = 3). *P < 0.05, *vs.* sham group; #P < 0.05, *vs.* SCII group (one-way analysis of variance). DAPI: 4′,6-Diamidino-2-phenylindole; NC: negative control; SCII: spinal cord ischemia/reperfusion injury; TUNEL: terminal deoxynucleotidyl transferase dUTP nick end labeling.

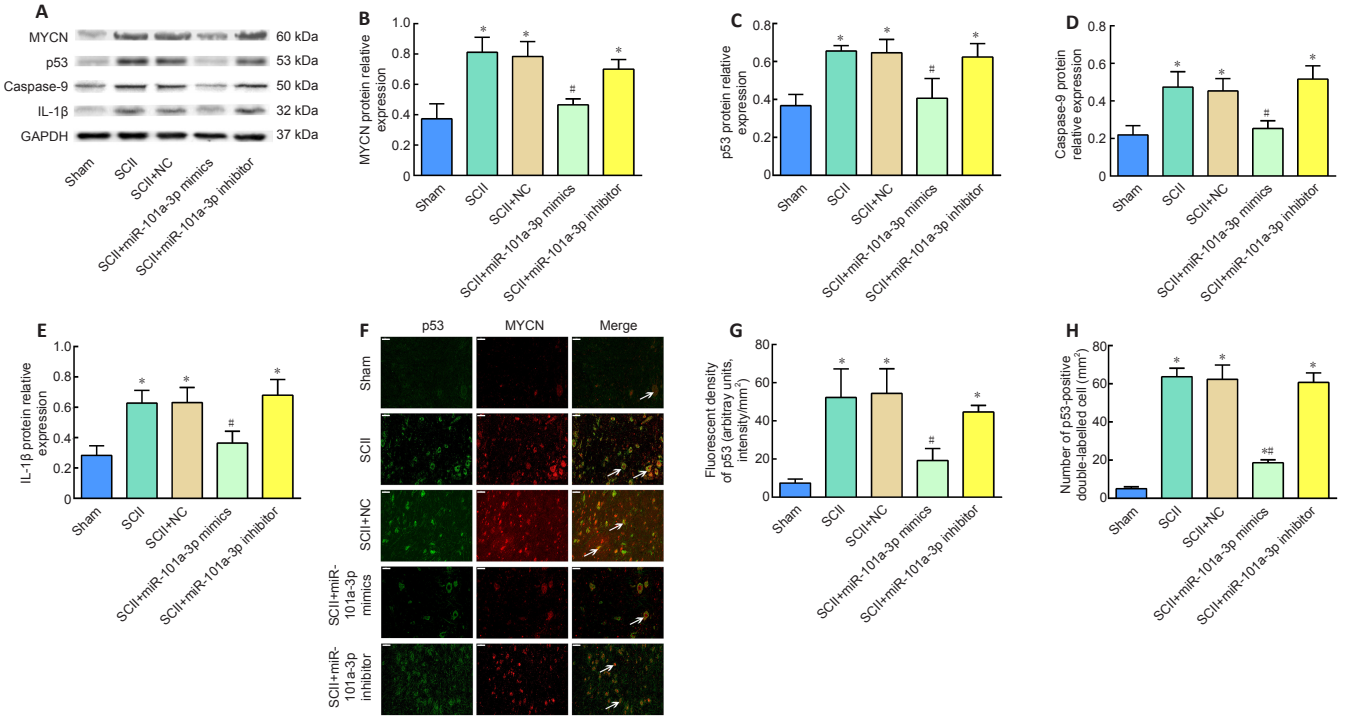

Figure 6 | The effect of synthetic miR-101a-3p on the MYCN-p53-caspase-9 signaling pathway and proinflammatory cytokine IL-1β at 24 hours after SCII.
(A) The expression of MYCN, p53, caspase-9 and IL-1β protein was assessed by western blot assay (n = 4 in each group). (B–E) Quantification of MYCN, p53, caspase-9 and IL-1β protein expression. The relative expression was normalized by GAPDH. (F) Double immunofluorescence staining indicated the colocalization (white arrow) of MYCN (red, Alexa Fluor 594) and p53 (green, fluorescein). Compared with the sham group, the SCII group showed stronger immunoreactivity of p53, and immunoreactivity in the miR-101a-3p mimic group was decreased compared with that in the SCII group. Scale bars: 50 μm, magnification, 40×. (G) Quantification of p53 immunoreactivity. (H) Number of p53/MYCN double-positive cells. The data are expressed as the mean ± SD (n = 3). *P < 0.05, *vs.* sham group; #P < 0.05, *vs.* SCII group (one-way analysis of variance). GAPDH: Glyceraldehyde-3-phosphate dehydrogenase; IL-1β: interleukin-1β; MYCN: v-myc myelocytomatosis viral-related oncogene; NC: negative control; NeuN: neuronal nuclei; SCII: spinal cord ischemia/reperfusion injury.

Discussion

The secondary damage of SCII can aggravate neuronal injury and induce serious dyskinesia (Li et al., 2014b, 2018b). Neuroapoptosis and inflammation are two important damaging mechanisms in this process (Chen et al., 2020). The present study demonstrated that elevated miR-101a-3p inhibited the MYCN-p53-caspase-9 pathway and cytokine IL-1β production, suggesting that the miR-101a-3p mimic improves neuronal injury by regulating neuroapoptosis and inflammation in SCII.

miR-101a-3p is regarded as a regulator in malignant cancer (Wang et al., 2010; Zhang et al., 2011). Recently, accumulating evidence has indicated that miR-101a plays important roles in acute kidney injury and cardiac injury. For example, miR-101 overexpression inhibits fibrosis and the epithelial-mesenchymal transition process, thereby impeding the progression of acute kidney injury to chronic kidney disease (Zhao et al., 2020). Additionally, the overexpression of miR-101a slowed the deterioration of cardiac function in rats after myocardial infarction and protected against the H_2O_2-induced cardiac ischemia/reperfusion (Pan et al., 2012; Zhai et al., 2020). Furthermore, miR-101a-3p plays a vital role in the CNS (Cohen et al., 2017; Zhang et al., 2019). The above findings show that miR-101a-3p could regulate neuroapoptosis and inflammation response. In this study, miR-101a-3p expression reduced over time and reached its lowest level at 24 hours after SCII, suggesting a connection between SCII and miR-101a-3p. Therefore, we performed the subsequent experiments at 24 hours. Our findings showed that the miR-101a-3p mimic ameliorated hind limb motor function and cell apoptosis and inhibited the MYCN-p53-caspase-9 signaling pathway and proinflammatory cytokine IL-1β production. The findings suggest that the miR-101a-3p mimic had a neuroprotective effect after SCII by regulating neuroapoptosis and inflammation.

MYCN encodes transcription factors controlling differentiation, proliferation, and apoptosis (Liu et al., 2016). It has been reported that MYCN is associated with kidney injury (Yakulov et al., 2018) and acrolein-induced acute lung injury (Leikauf et al., 2011). MYCN

also plays a critical role in hypoxic-ischemic encephalopathy (Jiang et al., 2018) and traumatic brain injury (Gupta and Prasad, 2016). In the CNS, MYCN is mostly distributed in the developing nervous system and mainly expressed in neuroectodermal progenitors under normal conditions (Zinin et al., 2014). MYCN dysfunction can inhibit expansion of neural progenitors (Knoepfler et al., 2002). In the present study, MYCN expression elevated over time and peaked at 24 hours, suggesting the involvement of MYCN in SCII. We also ascertained that miR-101a-3p directly targeted MYCN. Moreover, the miR-101a-3p mimic increased Tarlov scores and decreased the apoptosis rate of TUNEL-positive cells. To further study the effect of MYCN, we performed a double immunofluorescence assay to determine the distribution of MYCN in spinal cord. MYCN was mainly colocalized with NeuN but not with GFAP or Iba-1, suggesting that MYCN was at least partially upregulated in neurons. Together, these findings indicate that the miR-101a-3p mimic ameliorated hind limb motor dysfunction by inhibiting MYCN in neurons after SCII.

Our previous reports have confirmed that the p53 signaling pathway is involved in SCII (Li et al., 2018b). Additionally, it has been reported that p53 is directly targeted by MYCN (Chen et al., 2010; Agarwal et al., 2018). In this study, we suggested that miR-101a-3p/MYCN could have a neuroprotective effect after SCII by inhibiting the p53 signaling pathway. To study the mechanism, we investigated the MYCN-p53-caspase-9 signaling pathway by double immunofluorescence staining and western blot. Western blot indicated that the miR-101a-3p mimic greatly decreased protein expression levels of MYCN, p53 and caspase-9. Moreover, MYCN fluorescence was colocalized with p53 fluorescence at 24 hours after SCII, and the miR-101a-3p mimic decreased the number of cells double-labeled for MYCN and p53. Additionally, the results of the western blot were consistent with those of double immunofluorescence staining, indicating a close connection between MYCN, p53 and caspase-9. Our previous reports have shown that caspase-3 is involved in the p53-caspase-3 apoptotic pathway after SCII (Li et al., 2018b). Caspase-9 is also downstream of p53 and can activate caspase-3 to induce apoptosis (Czabotar et al., 2014; Sørensen et al., 2016). Protein expression of caspase-9 was greatly reduced by miR-101a-3p mimic in the present study. The production of proinflammatory cytokine IL-1β was also greatly decreased by the miR-101a-3p mimic. Together, these results suggest that the miR-101a-3p mimic protected against SCII-induced damage by inhibiting the MYCN-p53-caspase-9 signaling pathway and proinflammatory cytokine IL-1β production.

There are several limitations in our study. First, the sample size should be increased to improve the accuracy of this study. Second, more time points after SCII should be observed to better understand the neuroprotective effect of the miR-101a-3p mimic. Third, more *in vitro* cell experiments are needed to understand the molecular mechanisms in more detail.

In conclusion, this study examined the effect of miR-101a-3p and MYCN on regulating neuroapoptosis and inflammation after SCII. The findings indicate that the miR-101a-3p mimic ameliorates SCII-induced neuroapoptosis and inflammation by inhibiting MYCN and the p53 signaling pathway. Thus, miR-101a-3p upregulation could be a potential therapeutic treatment.

Author contributions: *Study design, study implementation and data collection: ZLZ, FSC; statistical analysis: ZLZ, DW, FSC; manuscript drafting: ZLZ, DW, FSC. All authors contributed to manuscript revision, read, and approved the submitted version of the manuscript.*
Conflicts of interest: *The authors report no conflicts of interest and are solely responsible for the content and writing of this manuscript.*

Open peer reviewer: *Renata Ciccarelli, University of Chieti-Pescara, Italy.*

References

Agarwal S, Milazzo G, Rajapakshe K, Bernardi R, Chen Z, Barbieri E, Koster J, Perini G, Coarfa C, Shohet JM (2018) MYCN acts as a direct co-regulator of p53 in MYCN amplified neuroblastoma. Oncotarget 9:20323-20338.

Astolfi A, Vendemini F, Urbini M, Melchionda F, Masetti R, Franzoni M, Libri V, Serravalle S, Togni M, Paone G, Montemurro L, Bressanin D, Chiarini F, Martelli AM, Tonelli R, Pession A (2014) MYCN is a novel oncogenic target in pediatric T-cell acute lymphoblastic leukemia. Oncotarget 5:120-130.

Bao N, Fang B, Lv H, Jiang Y, Chen F, Wang Z, Ma H (2018) Upregulation of miR-199a-5p protects spinal cord against ischemia/reperfusion-induced injury via downregulation of ECE1 in rat. Cell Mol Neurobiol 38:1293-1303.

Chava S, Reynolds CP, Pathania AS, Gorantla S, Poluektova LY, Coulter DW, Gupta SC, Pandey MK, Challagundla KB (2020) miR-15a-5p, miR-15b-5p, and miR-16-5p inhibit tumor progression by directly targeting MYCN in neuroblastoma. Mol Oncol 14:180-196.

Chen F, Li X, Li Z, Zhou Y, Qiang Z, Ma H (2020) The roles of chemokine (C-X-C motif) ligand 13 in spinal cord ischemia-reperfusion injury in rats. Brain Res 1727:146489.

Chen L, Iraci N, Gherardi S, Gamble LD, Wood KM, Perini G, Lunec J, Tweddle DA (2010) p53 is a direct transcriptional target of MYCN in neuroblastoma. Cancer Res 70:1377-1388.

Cohen JL, Jackson NL, Ballestas ME, Webb WM, Lubin FD, Clinton SM (2017) Amygdalar expression of the microRNA miR-101a and its target Ezh2 contribute to rodent anxiety-like behaviour. Eur J Neurosci 46:2241-2252.

Czabotar PE, Lessene G, Strasser A, Adams JM (2014) Control of apoptosis by the BCL-2 protein family: implications for physiology and therapy. Nat Rev Mol Cell Biol 15:49-63.

Gupta RK, Prasad S (2016) Age-dependent alterations in the interactions of NF-κB and N-myc with GLT-1/EAAT2 promoter in the pericontusional cortex of mice subjected to traumatic brain injury. Mol Neurobiol 53:3377-3388.

He F, Shi E, Yan L, Li J, Jiang X (2015) Inhibition of micro-ribonucleic acid-320 attenuates neurologic injuries after spinal cord ischemia. J Thorac Cardiovasc Surg 150:398-406.

He XY, Tan ZL, Mou Q, Liu FJ, Liu S, Yu CW, Zhu J, Lv LY, Zhang J, Wang S, Bao LM, Peng B, Zhao H, Zou L (2017) microRNA-221 Enhances MYCN via targeting nemo-like kinase and functions as an oncogene related to poor prognosis in neuroblastoma. Clin Cancer Res 23:2905-2918.

Jiang X, Yang J, Li H, Qu Y, Xu W, Yu H, Tong Y (2018) Huwe1 is a novel mediator of protection of neural progenitor L2.3 cells against oxygen-glucose deprivation injury. Mol Med Rep 18:4595-4602.

Khanna S, Rink C, Ghoorkhanian R, Gnyawali S, Heigel M, Wijesinghe DS, Chalfant CE, Chan YC, Banerjee J, Huang Y, Roy S, Sen CK (2013) Loss of miR-29b following acute ischemic stroke contributes to neural cell death and infarct size. J Cereb Blood Flow Metab 33:1197-1206.

Knoepfler PS, Cheng PF, Eisenman RN (2002) N-myc is essential during neurogenesis for the rapid expansion of progenitor cell populations and the inhibition of neuronal differentiation. Genes Dev 16:2699-2712.

Korshunov A, Schrimpf D, Ryzhova M, Sturm D, Chavez L, Hovestadt V, Sharma T, Habel A, Burford A, Jones C, Zheludkova O, Kumirova E, Kramm CM, Golanov A, Capper D, von Deimling A, Pfister SM, Jones DTW (2017) H3-/IDH-wild type pediatric glioblastoma is comprised of molecularly and prognostically distinct subtypes with associated oncogenic drivers. Acta Neuropathol 134:507-516.

Le MT, Shyh-Chang N, Khaw SL, Chin L, Teh C, Tay J, O'Day E, Korzh V, Yang H, Lal A, Lieberman J, Lodish HF, Lim B (2011) Conserved regulation of p53 network dosage by microRNA-125b occurs through evolving miRNA-target gene pairs. PLoS Genet 7:e1002242.

Leikauf GD, Concel VJ, Liu P, Bein K, Berndt A, Ganguly K, Jang AS, Brant KA, Dietsch M, Pope-Varsalona H, Dopico RA, Jr., Di YP, Li Q, Vuga LJ, Medvedovic M, Kaminski N, You M, Prows DR (2011) Haplotype association mapping of acute lung injury in mice implicates activin a receptor, type 1. Am J Respir Crit Care Med 183:1499-1509.

Li Q, Gao S, Kang Z, Zhang M, Zhao X, Zhai Y, Huang J, Yang GY, Sun W, Wang J (2018a) Rapamycin enhances mitophagy and attenuates apoptosis after spinal ischemia-reperfusion injury. Front Neurosci 12:865.

Li XQ, Wang J, Fang B, Tan WF, Ma H (2014a) Intrathecal antagonism of microglial TLR4 reduces inflammatory damage to blood-spinal cord barrier following ischemia/reperfusion injury in rats. Mol Brain 7:28.

Li XQ, Yu Q, Tan WF, Zhang ZL, Ma H (2018b) MicroRNA-125b mimic inhibits ischemia reperfusion-induced neuroinflammation and aberrant p53 apoptotic signalling activation through targeting TP53INP1. Brain Behav Immun 74:154-165.

Li XQ, Lv HW, Tan WF, Fang B, Wang H, Ma H (2014b) Role of the TLR4 pathway in blood-spinal cord barrier dysfunction during the bimodal stage after ischemia/reperfusion injury in rats. J Neuroinflammation 11:62.

Li XQ, Cao XZ, Wang J, Fang B, Tan WF, Ma H (2014c) Sevoflurane preconditioning ameliorates neuronal deficits by inhibiting microglial MMP-9 expression after spinal cord ischemia/reperfusion in rats. Mol Brain 7:69.

Li XQ, Chen FS, Tan WF, Fang B, Zhang ZL, Ma H (2017) Elevated microRNA-129-5p level ameliorates neuroinflammation and blood-spinal cord barrier damage after ischemia-reperfusion by inhibiting HMGB1 and the TLR3-cytokine pathway. J Neuroinflammation 14:205.

Lin Y, Liang X, Yao Y, Xiao H, Shi Y, Yang J (2019) Osthole attenuates APP-induced Alzheimer's disease through up-regulating miRNA-101a-3p. Life Sci 225:117-131.

Liu K, Wang S, Liu Y, Gu J, Gu S, Xu Z, Zhang R, Wang Z, Ma H, Chen Y, Ji L (2016) Overexpression of MYCN promotes proliferation of non-small cell lung cancer. Tumour Biol 37:12855-12866.

Liu SG, Wang YM, Zhang YJ, He XJ, Ma T, Song W, Zhang YM (2017) ZL006 protects spinal cord neurons against ischemia-induced oxidative stress through AMPK-PGC-1α-Sirt3 pathway. Neurochem Int 108:230-237.

Mestre C, Pélissier T, Fialip J, Wilcox G, Eschalier A (1994) A method to perform direct transcutaneous intrathecal injection in rats. J Pharmacol Toxicol Methods 32:197-200.

Padmanabhan R, Singh S (1979) Observations on the topographical relations of spinal nerve roots in the rat. Acta Anat (Basel) 105:378-380.

Pan Z, Sun X, Shan H, Wang N, Wang J, Ren J, Feng S, Xie L, Lu C, Yuan Y, Zhang Y, Wang Y, Lu Y, Yang B (2012) MicroRNA-101 inhibited postinfarct cardiac fibrosis and improved left ventricular compliance via the FBJ osteosarcoma oncogene/transforming growth factor-β1 pathway. Circulation 126:840-850.

Peifer M, Fernández-Cuesta L, Sos ML, George J, Seidel D, Kasper LH, Plenker D, Leenders F, Sun R, Zander T, Menon R, Koker M, Dahmen I, Müller C, Di Cerbo V, Schildhaus HU, Altmüller J, Baessmann I, Becker C, de Wilde B, et al. (2012) Integrative genome analyses identify key somatic driver mutations of small-cell lung cancer. Nat Genet 44:1104-1110.

Percie du Sert N, Hurst V, Ahluwalia A, Alam S, Avey MT, Baker M, Browne WJ, Clark A, Cuthill IC, Dirnagl U, Emerson M, Garner P, Holgate ST, Howells DW, Karp NA, Lazic SE, Lidster K, MacCallum CJ, Macleod M, Pearl EJ, et al. (2020) The ARRIVE guidelines 2.0: Updated guidelines for reporting animal research. PLoS Biol 18:e3000410.

Roshan R, Shridhar S, Sarangdhar MA, Banik A, Chawla M, Garg M, Singh VP, Pillai B (2014) Brain-specific knockdown of miR-29 results in neuronal cell death and ataxia in mice. RNA 20:1287-1297.

Roy B, Beamon J, Balint E, Reisman D (1994) Transactivation of the human p53 tumor suppressor gene by c-Myc/Max contributes to elevated mutant p53 expression in some tumors. Mol Cell Biol 14:7805-7815.

Saika R, Sakuma H, Noto D, Yamaguchi S, Yamamura T, Miyake S (2017) MicroRNA-101a regulates microglial morphology and inflammation. J Neuroinflammation 14:109.

Sørensen BH, Nielsen D, Thorsteinsdottir UA, Hoffmann EK, Lambert IH (2016) Downregulation of LRRC8A protects human ovarian and alveolar carcinoma cells against Cisplatin-induced expression of p53, MDM2, p21Waf1/Cip1, and Caspase-9/-3 activation. Am J Physiol Cell Physiol 310:C857-873.

Sun G, Lu J, Zhang C, You R, Shi L, Jiang N, Nie D, Zhu J, Li M, Guo J (2017) MiR-29b inhibits the growth of glioma via MYCN dependent way. Oncotarget 8:45224-45233.

Wang D, Chen F, Fang B, Zhang Z, Dong Y, Tong X, Ma H (2020a) MiR-128-3p alleviates spinal cord ischemia/reperfusion injury associated neuroinflammation and cellular apoptosis via SP1 suppression in rat. Front Neurosci 14:609613.

Wang H, Yu Q, Zhang ZL, Ma H, Li XQ (2020b) Involvement of the miR-137-3p/CAPN-2 interaction in ischemia-reperfusion-induced neuronal apoptosis through modulation of p35 cleavage and subsequent caspase-8 overactivation. Oxid Med Cell Longev 2020:2616871.

Wang HJ, Ruan HJ, He XJ, Ma YY, Jiang XT, Xia YJ, Ye ZY, Tao HQ (2010) MicroRNA-101 is down-regulated in gastric cancer and involved in cell migration and invasion. Eur J Cancer 46:2295-2303.

Wang L, Yao Y, He R, Meng Y, Li N, Zhang D, Xu J, Chen O, Cui J, Bian J, Zhang Y, Chen G, Deng X (2017) Methane ameliorates spinal cord ischemia-reperfusion injury in rats: Antioxidant, anti-inflammatory and anti-apoptotic activity mediated by Nrf2 activation. Free Radic Biol Med 103:69-86.

Wei JS, Song YK, Durinck S, Chen QR, Cheuk AT, Tsang P, Zhang Q, Thiele CJ, Slack A, Shohet J, Khan J (2008) The MYCN oncogene is a direct target of miR-34a. Oncogene 27:5204-5213.

Yakulov TA, Todkar AP, Slanchev K, Wiegel J, Bona A, Groß M, Scholz A, Hess I, Wurditsch A, Grahammer F, Huber TB, Lecaudey V, Bork T, Hochrein J, Boerries M, Leenders J, de Tullio P, Jouret F, Kramer-Zucker A, Walz G (2018) CXCL12 and MYC control energy metabolism to support adaptive responses after kidney injury. Nat Commun 9:3660.

Zhai C, Hu H, Tang G, Pan H, Zhang Y, Qian G (2020) MicroRNA-101a protects against the H(2)O(2)-induced injury on cardiomyocytes via targeting BCL2L11. Am J Transl Res 12:2760-2768.

Zhang JG, Guo JF, Liu DL, Liu Q, Wang JJ (2011) MicroRNA-101 exerts tumor-suppressive functions in non-small cell lung cancer through directly targeting enhancer of zeste homolog 2. J Thorac Oncol 6:671-678.

Zhang L, Yan J, Liu Q, Xie Z, Jiang H (2019) LncRNA Rik-203 contributes to anesthesia neurotoxicity via microRNA-101a-3p and GSK-3β-mediated neural differentiation. Sci Rep 9:6822.

Zhang Z, Li X, Chen F, Li Z, Wang D, Ren X, Ma H (2021) Downregulation of LncRNA Gas5 inhibits apoptosis and inflammation after spinal cord ischemia-reperfusion in rats. Brain Res Bull 168:110-119.

Zhao JY, Wang XL, Yang YC, Zhang B, Wu YB (2020) Upregulated miR-101 inhibits acute kidney injury-chronic kidney disease transition by regulating epithelial-mesenchymal transition. Hum Exp Toxicol 39:1628-1638.

Zhou Y, Shiok TC, Richards AM, Wang P (2018) MicroRNA-101a suppresses fibrotic programming in isolated cardiac fibroblasts and in vivo fibrosis following trans-aortic constriction. J Mol Cell Cardiol 121:266-276.

Zindy F, Knoepfler PS, Xie S, Sherr CJ, Eisenman RN, Roussel MF (2006) N-Myc and the cyclin-dependent kinase inhibitors p18Ink4c and p27Kip1 coordinately regulate cerebellar development. Proc Natl Acad Sci U S A 103:11579-11583.

Zinin N, Adameyko I, Wilhelm M, Fritz N, Uhlén P, Ernfors P, Henriksson MA (2014) MYC proteins promote neuronal differentiation by controlling the mode of progenitor cell division. EMBO Rep 15:383-391.

P-Reviewer: Ciccarelli R; C-Editor: Zhao M; S-Editors: Yu J, Li CH; L-Editors: McCollum L, Yu J, Song LP; T-Editor: Jia Y